Formation of the High-Spin S_2 State Related to the Extrinsic Proteins in the Oxygen Evolving Complex of Photosystem II

Shota Taguchi[†], Liangliang Shen[$], Guangye Han[$], Yasufumi Umena[#‡], Jian-Ren Shen[$#], Takumi Noguchi[†] and Hiroyuki Mino[†]*

[†] Division of Material Science, Graduate School of Science, Nagoya University, Furo-cho, Chikusa-ku, 464-8602, Nagoya, Aichi, Japan; [$]Photosynthesis Research Center, Key Laboratory of Photobiology, Institute of Botany, Chinese Academic Science, China; [#]Research Institute for Interdisciplinary Science, and Graduate School of Natural Science and Technology, Okayama University, Okayama, Japan

Corresponding Author *E-mail:mino@bio.phys.nagoya-u.ac.jp

Present Address [‡]Division of Biophysics, Department of Physiology, Jichi Medical University, Shimotsuke, Tochigi, 329-0498, Japan

Abstract

The high-spin S_2 state was investigated with photosystem II (PSII) from spinach, *Thermosynechococcus vulcanus*, and *Cyanidioschyzon merolae*. In extrinsic proteins-depleted PSII, high-spin electron paramagnetic resonance (EPR) signals were detected in neither species, whereas all species showed $g \sim 5$ signals in the presence of a high-concentration of Ca^{2+} instead of the multiline signal. In the intact and PsbP/Q-depleted PSII from spinach, the $g = 4.1$ EPR signal was detected. These results show that formation of the high-spin S_2 state of the manganese cluster is regulated by the extrinsic proteins through a charge located near the Mn4 atom in the Mn_4CaO_5 cluster, but is independent of the intrinsic proteins. The shift to the $g \sim 5$ state is caused by tilting of the z-axis in the Mn4 coordinates through hydrogen bonds or external divalent cations. The structural modification may allow insertion of an oxygen atom during the S_2-to-S_3 transition.

TOC GRAPHICS

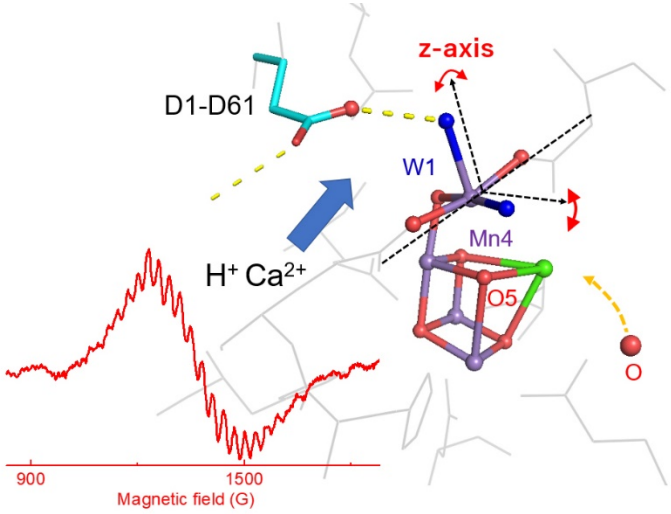

In 4.6 billion years of the history of the earth, the invention of photosynthetic oxygen evolution is one of the most dramatic events, which allowed formation of the oxygenic atmosphere that provides the basis for life activities. The Mn_4CaO_5 cluster, which is located in the photosystem II (PSII) protein complex,[1-3] is the core machinery for the oxygen evolution. Various photosynthetic species have spread all over the earth. On the other hand, the Mn_4CaO_5 cluster is well-conserved in all oxygen-evolving photosynthetic species. Figure 1 shows the evolution of oxygen-evolving species, which was simplified into five groups; cyanobacteria, green algae, green plants, red algae, and diatoms. Cyanobacteria are the ancestor of both red and green lineages (Figure 1). Red algae and diatoms are grouped into the red lineage, whereas green algae and plants are grouped into the green lineage. The main differences of these species are the variety of the extrinsic proteins located at the membrane surface of the lumenal side,[4, 5] which are essential for the oxygen-evolving activity. Cyanobacteria have three major extrinsic proteins, PsbO, PsbV, and PsbU, while red algae and diatoms have PsbQ' and PsbQ'/Psb31, respectively, in addition to the PsbO/V/U. In contrast, green algae and plants have PsbO, PsbP, and PsbQ as their major extrinsic proteins (Figure 1). X-ray crystallography and cryo-electron microscopy have revealed the structures of PSII from different photosynthetic organisms (Figure. S1).[6-10]

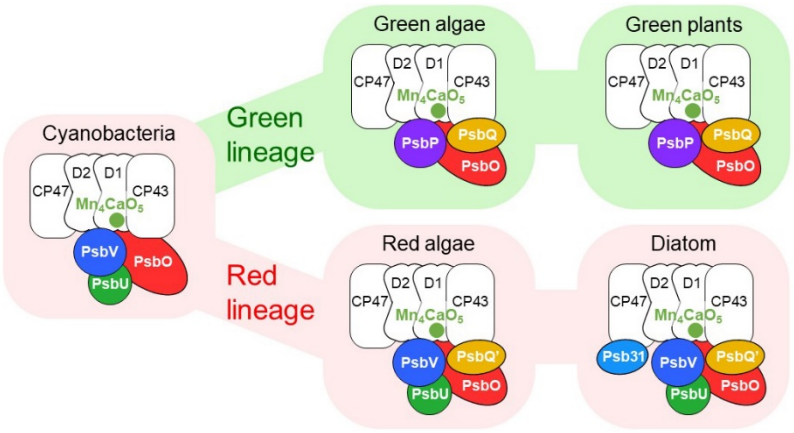

Figure 1. Illustration of the evolution of PSII. All the systems have D1/D2/CP47/CP43 as intrinsic proteins. Green algae and green plants in the green lineage have PsbO/P/Q as extrinsic proteins. Cyanobacteria, red algae, and diatoms in the red lineage have conserved PsbO/V/U, although red algae has PsbQ' and diatoms has PsbQ'/Psb31 as extra extrinsic proteins.

The manganese cluster has five different redox states denoted S_n ($n = 0 – 4$), where S_n advances to S_{n+1} by one-electron oxidation. S_4 is the highest oxidation state of the cluster, and it immediately relaxes to the lowest oxidation state S_0, with the evolution of molecular oxygen.[11] The structure of the Mn_3CaO_4 cube and an additional Mn and oxygen resemble a 'distorted chair' (Figure S2).[6]

The Mn-cluster has been studied mainly using plant and cyanobacterial PSII. Electron paramagnetic resonance (EPR) studies have shown some structural differences between plants and cyanobacteria. In plant PSII, an EPR signal is detected in the S_1 state using a parallel polarization mode, showing a broad and featureless signal centered at $g = 4.8$ while cyanobacterial PSII shows a hyperfine structure spacing with 32 G at $g = 12$ in the S_1 state.[12, 13] The extrinsic PsbO/P/Q-depleted spinach PSII also gives the S_1 state spectrum with a similar hyperfine structure at $g = 12$.[13] The results show that the extrinsic proteins give rise to some structural modifications to the Mn_4CaO_5 cluster directly. The differences between plant and cyanobacterial PSII are observed in the S_2 state more clearly. In the S_2 state of plant PSII, two kinds of isomers are detected, the $g = 2$ multiline and the $g = 4.1$ signals. However, the $g = 4.1$ EPR signal is not detected in cyanobacterial PSII under normal conditions.

The amino acid residues around the manganese cluster are well conserved among different species, and the difference between plants and cyanobacteria seems to be only the Asp87 residue

of the D1 subunit (D1-N87). Banerjee et al. reported that a D1-N87A mutant of the cyanobacterium *Synechocystis* sp. PCC 6803 showed no $g = 4$ signal,[14] suggesting that D1-N87 has no relationship with the conversion between the $g = 2$ multiline and $g = 4$ signals. This is consistent with the results in *Chlamydomonas reinhardtii*, which has the same asparagine residue as that in cyanobacteria, but the $g = 4$ signal was observed.[15] Therefore, the difference between plant and cyanobacterial PSII is speculated to be ascribed to the difference in the extrinsic proteins.

So far, four kinds of S_2-state signals have been reported: the $g = 2$ multiline, $g = 4.1$, $g = 6$-10, and $g = 5$ signals. The $g = 6$-10 signal is converted from the $g = 2$ multiline signal by near-infrared illumination below 65 K.[16] The $g = 5$ signal has been proposed to arise from an intermediate state between the $g = 4$ S_2 state and the S_3 state.[17-20] Although some quantum chemical calculations have been reported,[21, 22] the four spin model based on the calculations does not reproduce the EPR results.

Recently, we have shown that the *g*-factor was shifted from 4 to 5 in the PsbO/P/Q-depleted spinach PSII, depending on the concentrations of divalent cations.[23] The results showed that the g factor shift is caused by the structural modification of the W1-Mn4-O5 axis in the manganese cluster.[23] The $g = 5$ signal increases in proportion to the concentration of Ca^{2+}, where the $g = 5$ and the multiline signal are in equilibrium.[23] The relationship between the formation of the O-O bond beyond the S_3 state and the high spin structures in the S_2 state is important to understand the whole mechanism of the oxygen-evolving reactions. In this paper, we studied the role of the extrinsic proteins in the regulation of the high spin state in the S_2 state from different species of organisms.

Figure 2 shows the EPR spectra of (a) untreated, (b) PsbP/Q-depleted and (c, d) PsbO/P/Q-depleted spinach PSII in the presence of (a-c) 5 mM and (d) 1 M $CaCl_2$. The removal of the

extrinsic proteins from each PSII was conducted by 2 M NaCl or 1 M $CaCl_2$ treatment as shown in Figure S3. The spectra were obtained by subtraction of the S_1-state spectra from the S_2-state spectra that were obtained by illumination at 200 K and subsequent annealing at 273 K. The g = 4-5 signal was enhanced by annealing.[23] In the absence of PsbP/Q, the g = 4.1 signal was detected with a reduced intensity. In the absence of PsbO/P/Q, the g = 4 signal was hardly detected. The result shows that the formation of the g = 4.1 signal is ascribed to the presence of PsbO. In addition, it was shown that high-concentration of Ca^{2+} induced the g = 5 signal instead of the multiline signal.[23]

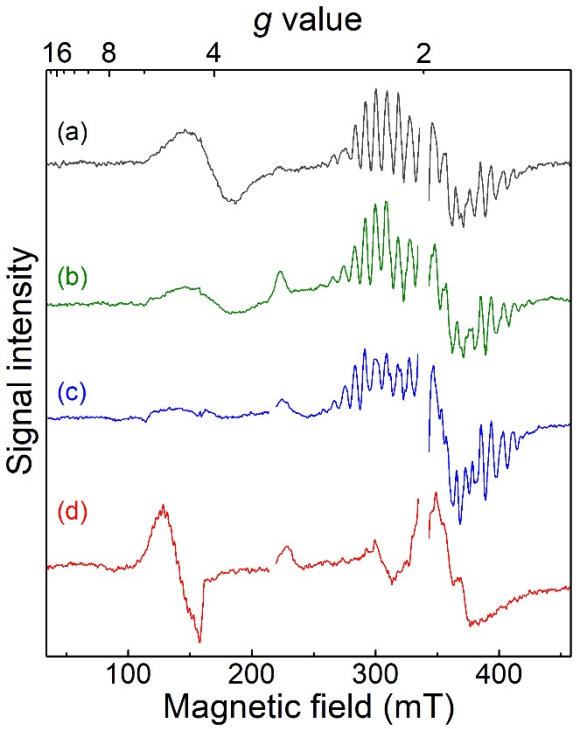

Figure 2. EPR spectra of the spinach PSII of (a) untreated, (b) PsbP/Q-depleted, and (c, d) PsbO/P/Q-depleted PSII in the presence of (a-c) 5 mM and (d) 1 M $CaCl_2$. The S_1-state spectra were subtracted from the S_2-state spectra obtained after annealing at 273 K. Experimental

conditions: microwave frequency, 9.49 GHz; microwave power, 0.64 mW, modulation frequency, 100 kHz; modulation amplitude, 9 G.

Figure 3 shows the EPR spectra of (a) untreated and (b, c) PsbO/V/U or PsbO/V/U/Q'-depleted PSII in the presence of (a, b) 5 mM and (c) 1 M $CaCl_2$ from (A) *T. vulcanus* and (B) *C. merolae*. In both PSII, the $g = 4$ signal was detected in neither untreated nor extrinsic proteins-depleted PSII. However, in the presence of 1 M $CaCl_2$, the high-spin signal was observed at $g = 4.85$ and $g = 4.90$ in PSII from *T. vulcanus* and *C. merolae*, respectively, instead of the multiline signal. These results show that there is a species dependence in the formation of the S_2 isomers under the usual condition, but this species dependence disappears in the absence of the extrinsic proteins.

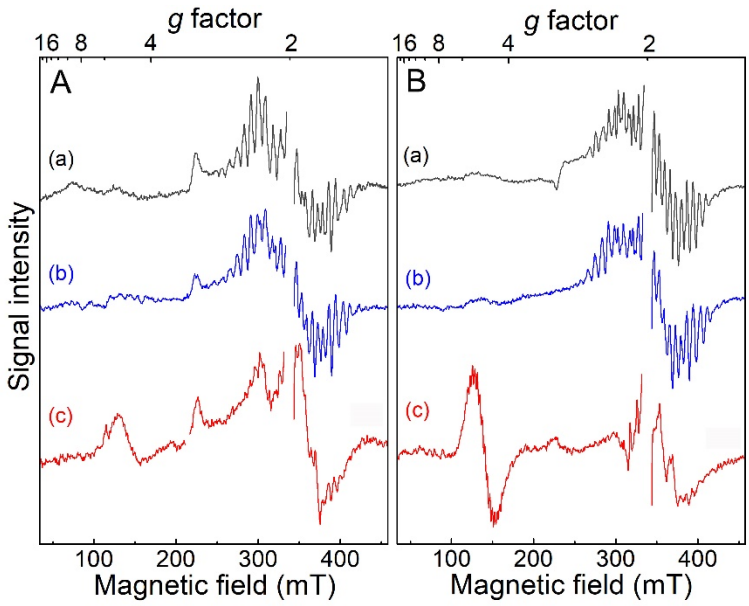

Figure 3. EPR spectra of (a) untreated and (b, c) PsbO/V/U or PsbO/V/U/Q'-depleted PSII from (A) *T. vulcanus* and (B) *C. merolae*. Samples contain (a, b) 5 mM and (c) 1 M $CaCl_2$. The S_1-

state spectra were subtracted from the S_2-state spectra obtained after annealing at 290 K. The experimental conditions are the same as that for Figure 2.

In the absence of the extrinsic proteins, the g = 5 signals were observed in all the species in the presence of high concentrations of divalent cations, whereas the multiline signal was disappeared under such conditions. Figure 4 shows the expanded spectra of the g = 5 signals in the different species. Trace b was obtained at pH 8.6 in the *T. vulcanus* PSII, corresponding to the condition previously used for detection of the similar signal in *T. elongatus* PSII.[17, 18] Traces c-e were obtained in the extrinsic proteins-depleted PSII at pH 6.0 from spinach (c), *T. vulcanus* (d), and *C. merolae* (e). The subtraction procedures are shown in Figures S4 and S5. Some differences in the g-value may be due to the sharpness of the hyperfine peaks. The properties of the g = 4-5 signals were listed in Table 1.

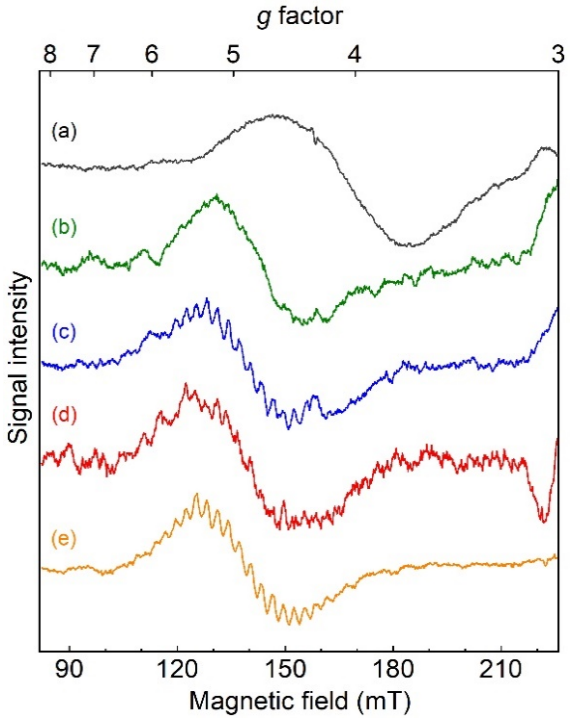

Figure 4. High-spin S_2 EPR signals of PSII in the S_2 state after annealing at 273-290 K. Each spectrum was obtained by subtraction of the S_1-state spectra or S_2-state spectra before annealing to eliminate the unwanted spike signal at $g \sim 4.3$. Spectra were recorded with (a) untreated PSII membranes from spinach at pH 6.0, (b) PSII core complexes from *T. vulcanus* at pH 8.6, and (c-e) $CaCl_2$-treated PSII in the presence of 1 M $CaCl_2$ at pH 6.0 from (c) spinach, (d) *T. vulcanus*, and (e) *C. merolae*. Experimental condition is the same as that for Figure 3.

Table1. EPR properties of the g = 4-5 signals in PSII.

	g-value	Line width (mT)	Hyperfine spacing (mT)
Spinach (PsbO/P/Q-depleted)	4.86	22.8	3.1 ± 0.3
T. vulcanus (PsbO/V/U-depleted)	4.85	28.7	2.9 ± 0.2
C. merolae (PsbO/V/U/Q'-depleted)	4.90	25.5	3.0 ± 0.3
Spinach (untreated)	4.09	38.9	n.d.
T. vulcanus (untreated, pH 8.6)	4.74	23.9	n.d.

The model structures of the S_2-state isomers related to the extrinsic proteins are summarized in Figure S6, which are based on the recent model for the $g \sim 5$ state.[23] In this model, the high-spin S_2 state is stabilized by a charge effect near the manganese cluster.[23] The decrease of the $g \sim 4$ signal in the PsbP/Q-depleted PSII reflects the roles of these extrinsic proteins for maintaining Ca^{2+} and Cl^-.[5] Furthermore, depletion of PsbO causes the complete loss of the $g \sim 4$ signal in the spinach PSII. Although the size of PsbO depends on the species, it is possible to compare the PsbO surfaces in the lumenal side among the different species using the crystal structure and the

alignment of the amino-acid sequences. The surface charge distribution of the PsbO is similar among the different species. Differences in the PsbO protein are found in the region in contact with CP47 among the species, and the region in contact with the O4 path contacting with D1-N87. The D1-N87 have been already excluded from the possibility.[14, 15] Therefore, we compared the sequences of PsbO in the CP47-binding region in different species (Table S1). Although red algal and cyanobacterial PSII have PsbO, they do not show the g = 4 signal. In this region, the differences in the amino acid residues between species seem to exist only at the residue of R262 in plants (Figure S7). PsbO-R262 is conserved in higher plants and *C. reinhardtii*, but varies significantly in cyanobacteria and red algae. In some cyanobacteria, this residue is missing, but in other cyanobacteria and red algae, it is changed to Q, A or E (Table S1). PsbO-R262 located at the end of the region in spinach does not form a salt-bridge due to the lack of a negatively charged amino acid residue. The shift of the g = 4 signal toward g = 5 is ascribed to a charge effect near the manganese cluster.[23] However, as R262 is far from the manganese cluster by more than 10 Å, it may not provide a direct effect. PsbO-R262 interacts with the manganese cluster via a hydrogen-bond network through D1-D61 extending from PsbO to the PSII core proteins (Figure S8). D1-D61 is one of the candidates for charged residues deriving the structural modifications.[18, 24] The network also includes the Cl^- site, which also affects the formation of the high-spin state.[25-27] If PsbO-R262 is related to the protonation of D1-D61,[18] the g ~5 state might be induced through the charge of PsbO involved in the hydrogen-bond network.

In the following, we consider the physical implications of the g ~5 signal in the structure and mechanism of oxygen evolution. The spin Hamiltonian is generally expressed as:

$$\mathcal{H} = g\beta \boldsymbol{S}\boldsymbol{B_0} + \sum \boldsymbol{I}\cdot\boldsymbol{A}\cdot\boldsymbol{S} + D\left[\boldsymbol{S_z^2} - \frac{1}{3}S(S+1)\right] + E\,(\boldsymbol{S_x^2} - \boldsymbol{S_y^2}) \qquad (1)$$

, where $\boldsymbol{S}$ and $\boldsymbol{I}$ are electron spin and nuclear spin operators, D and E are zero-field splitting parameters, g is an intrinsic g-factor of ~2, $\boldsymbol{A}$ is a hyperfine tensor, and $\boldsymbol{S}$ is an effective spin operator ($\boldsymbol{S_x}$, $\boldsymbol{S_y}$, $\boldsymbol{S_z}$), and $\boldsymbol{B_0}$ is an external magnetic field. The effective g factor is determined by the intrinsic g-factor and zero-field splitting by the interaction with the orbital angular momentum. The zero-field splitting consists of each onsite fine structure (d) of a manganese ion and the interactions between the ions. The angular dependence of the $g = 4$ signal shows that the zero-field splitting of the signal is mainly ascribed to 'Mn4',[29] indicating that the shift of the effective g-factor can also be ascribed to 'Mn4'. In the d-orbital system of the transition metal, the spin-orbital interaction was quenched under the symmetrical coordinates around the z-axis, i.e., d_{z2} and d_{x2-y2} orbitals (Figure S8). Figure 5 shows the structural model for the modification of the $g \sim 4$ to the $g \sim 5$ signal. The xyz-axes in Figure 5 are defined in eq. (1), and the orientation of the z-axis is determined by our previous results.[29] Mn4 is surrounded by the 6 oxygen atoms in the usual S_2 state [6, 30]. Therefore, the intrinsic g-factor is close to be $g = 2$,[29] where the effective $g \sim 4$ signal in the $\boldsymbol{S} = 5/2$ state is detected by the combination of the zero-field splitting. On the other hand, the $g \sim 5$ signal arises from the $\boldsymbol{S} = 5/2$ or $\boldsymbol{S} = 7/2$ spin system.[23]

In the case of the $\boldsymbol{S} = 5/2$ spin system, the breakage of the orthorhombic symmetry would cause the shift from the intrinsic $g \sim 2$ (Figure S8), where the z-axis for the crystalline field is along the Mn4-W1 axis, where W1 is the oxygen of the water molecule. The breakage of the Mn4-O5 coupling is also required for the formation of the $\boldsymbol{S} = 7/2$ spin system. In both cases of $\boldsymbol{S} = 5/2$ and 7/2, the modification of the W1-Mn4-O5 axis is required for the $g \sim 5$ signal. Quantum chemical calculations suggest that the Mn4-O5 distance is easily elongated.[21, 31] The D1-D61 residue is connected to the Mn4 via the water molecule W1. Besides, the y-axis is relatively fixed on the line of the amino-acid residues, D1-D170 and D1-E333. It is notable that the y-axis of Mn4 has the

unique linear coordinates with the amino acid residues for a manganese atom in the cluster. Therefore, a tilt of the *z*-axis is essential for the interaction with W1. D1-D61 connects to PsbO-R262 through a hydrogen-bond network. The perturbation of the hydrogen-bond of D1-D61 to Mn4 explains the pH dependence of the $g \sim 5$ signal.[18] An external cation would also influence the hydrogen-bond of D1-D61 in the extrinsic proteins-depleted PSII. These interactions pull the Mn4, which causes the distortion of the *z*-axis from the octahedral coordinates.

The manganese cluster in the S_2 state is composed of one Mn(III) and three Mn(IV) ions. The onsite zero-field splitting (*d*) of Mn(III) has been expected to be one order of magnitude larger than that of Mn(IV).[28] However, recent studies suggested that Mn(IV) ion has a larger zero-field splitting.[32] In a recent report, we measured the orientational dependence of the $g = 4$ signal and compared with the crystal structure.[29] The results showed that the main zero-field splitting is ascribed to the Mn4, but not to Mn1.[29] It is notable that this experimental result is independent of the valence of Mn4.

Quantum chemical calculations have shown the two possibilities of Mn1 (III) and Mn4(III) in the S_2 high-spin state. The Mn1(III) model gives a set of smaller values of the exchange couplings *J*,[22, 33] which would be inadequate for the formation of the $g = 4 - 5$ signals in the four coupled spin model. From this point of view, the original Mn4(III) model with a set of larger exchange couplings[21, 34] would be more preferable. Further studies would be required to clarify these models.

Recent XRD results show the insertion of an oxygen atom during the transition from the S_2 to S_3 states.[35-37] The insertion of the oxygen atom is one of the most important reactions to solve the oxygen evolving mechanism. The regulation of the coordination geometry through the charge of D1-D61 would be a key reaction for the structural modification of the cluster.

In conclusion, the species dependence of the high-spin S_2 state was investigated in spinach, *T. vulcanus*, and *C. merolae* PSII. The g = 4.1 signal was observed in intact and PsbP/Q-depleted spinach PSII, but not in the *T. vulcanus* and *C. merolae* PSII. In the extrinsic proteins-depleted PSII from these species, no high-spin signal was detected under a low concentration of Ca^{2+}, but in the presence of a high-concentration of Ca^{2+}, the g ~ 5 signals were detected in all of these species instead of the multiline signal. These results show that the formation of the high-spin S_2 state is regulated by the extrinsic proteins, but independent of the species-dependence of the intrinsic proteins. The charge near Mn4 may cause the distortion of the coordinates of Mn4 along the *z*-axis, and allows the insertion of an oxygen atom through a hydrogen-bond network. The results will provide a clue to clarify the role of the extrinsic proteins in the molecular mechanism of the S-state transitions and water oxidation.

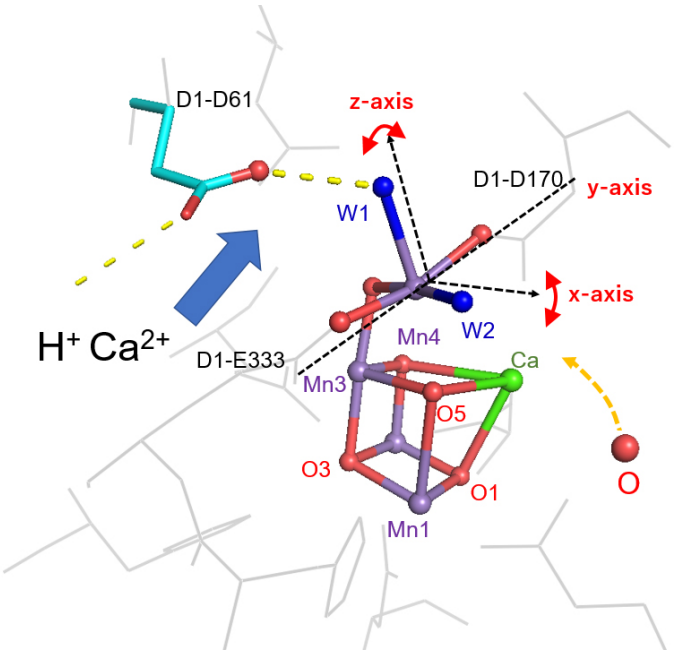

Figure 5. Structural model of the modification of the g = 4 to the g = 5 state. The xyz-axes are defined in eq. (1).[29] Access of cations toward D1-D61 gives the perturbation of the z-axis of Mn4 in the S_2 high-spin state, resulting in the formation of the g = 5 signal.

Experimental Methods

PSII membranes were prepared from market spinach according to the method described previously.[23] The membranes were suspended in a buffer containing 400 mM sucrose, 5 mM NaCl, 5 mM $CaCl_2$, 0.5 mM EDTA•2Na and 40 mM Mes/NaOH (pH 6.0) after centrifugation at 43,000 *x* g for 20 min. PSII core complexes were prepared from *Thermosynechococcus vulcanus* [6, 38] and *Cyanidioschyzon merolae*.[8, 39] The purified core complexes were suspended in the same buffer as that used for the PSII membranes after centrifugation at 20,000×g for 10 min in the presence of 10% PEG6,000. All treatments were performed under dim green light at 4ºC.

Depletion of the extrinsic proteins, PsbP/Q, in spinach PSII, was performed by treatment with 2 M NaCl.[40] Depletion of PsbO/P/Q in spinach, PsbO/V/U in *T. vulcanus*, and PsbO/V/U/Q' in C. merolae, was performed by 1 M $CaCl_2$ treatment.[41] The extrinsic proteins-depleted samples were resuspended in the above Mes buffer (pH 6.0). For experiments with a high-concentration of cation, the samples were resuspended with the same buffer but containing 1 M $CaCl_2$. The S_2 state was formed by white light illumination (500 W tungsten lamp) for 3 min for core complexes and 5 min for membranes at 200 K. After illumination, samples were annealed in darkness for approximately 2 seconds at 290 K for core complexes and 273 K for membranes.[18, 23]

X-band CW-EPR measurements were carried out using a Bruker 300E EPR spectrometer with a super high Q resonator (ER 4122SHQ) and a gas flow temperature control system (ESR900, Oxford Instruments, Oxford, GB). All EPR measurements were performed at 6 K.

Supporting Information.

Figure S1: X-ray crystallographic and cryo-electron microscopic structures of PSII protein complexes, **Figure S2**: The structure of the water oxidizing center of photosystem II, **Figure S3**: SDS-PAGE analysis of the PSII membranes from spinach and the PSII core complexes isolated from *T. vulcanus* and *C. merolae*, **Figure S4**: EPR spectra of PsbO/V/U-depleted PSII from *T. vulcanus* in the presence of 1 M $CaCl_2$, **Figure S5**: EPR spectra of PsbO/V/U/Q'-depleted PSII from *C. merolae* in the presence of 1 M $CaCl_2$; **Figure S6**: The model of the relationship between the manganese cluster and the extrinsic proteins; **Figure S7**: Protein structure of PsbO around the CP47-binding region**, Figure S8**: The relationship between *d* electrons in the crystalline field and the *g*-factor. **Table S1**: The alignment of the protein sequences of PsbO in the CP47-binding region in different species.

Author Contributions

The manuscript was written through the contributions of all authors. / All authors have approved the final version of the manuscript.

Notes

The authors declare no competing financial interest.

ACKNOWLEDGMENTS

This work was partly supported by a Nanotechnology Platform Program <Molecule and Material Synthesis> (JPMXP0S20MS1007) of the Ministry of Education, Culture, Sports, Science and Technology (MEXT), Japan (to H.M), JSPS KAKENHI Grant Number JP20H05096 (to H.M.), JP17H06435, JP17H03662, JP17H06433 (to T.N.), and a National Key R&D Program of China (2017YFA0503700), a National Natural Science Foundation of China (31470339), a Strategic Priority Research Program of the Chinese Academy of Sciences (XDB17000000).

REFERENCES

(1) McEvoy, J. P.; Brudvig, G. W. Water-splitting chemistry of photosystem II. *Chem. Rev.* **2006,** *106*, 4455-4483.
(2) Shen, J. R. The Structure of Photosystem II and the Mechanism of Water Oxidation in Photosynthesis. *Annu. Rev. Plant Biol.* **2015,** *66*, 23-48.
(3) Lubitz, W.; Chrysina, M.; Cox, N. Water oxidation in photosystem II. *Photosynth. Res.* **2019**.
(4) Enami, I.; Okumura, A.; Nagao, R.; Suzuki, T.; Iwai, M.; Shen, J. R. Structures and functions of the extrinsic proteins of photosystem II from different species. *Photosynth. Res.* **2008,** *98*, 349-363.
(5) Ifuku, K.; Noguchi, T. Structural Coupling of Extrinsic Proteins with the Oxygen-Evolving Center in Photosystem II. *Front. Plant Sci.* **2016,** *7*, 84.
(6) Umena, Y.; Kawakami, K.; Shen, J. R.; Kamiya, N. Crystal structure of oxygen-evolving photosystem II at a resolution of 1.9 Å. *Nature* **2011,** *473*, 55-60.
(7) Wei, X. P.; Su, X. D.; Cao, P.; Liu, X. Y.; Chang, W. R.; Li, M.; Zhang, X. Z.; Liu, Z. F. Structure of spinach photosystem II-LHCII supercomplex at 3.2 Å resolution. *Nature* **2016,** *534*, 69-74.
(8) Ago, H.; Adachi, H.; Umena, Y.; Tashiro, T.; Kawakami, K.; Kamiya, N.; Tian, L. R.; Han, G. Y.; Kuang, T. Y.; Liu, Z. Y., *et al.* Novel Features of Eukaryotic Photosystem II Revealed by Its Crystal Structure Analysis from a Red Alga. *J. Biol. Chem.* **2016,** *291*, 5676-5687.
(9) Pi, X.; Zhao, S. H.; Wang, W. D.; Liu, D. S.; Xu, C. Z.; Han, G. Y.; Kuang, T. Y.; Sui, S. F.; Shen, J. R. The pigment-protein network of a diatom photosystem II-light-harvesting antenna supercomplex. *Science* **2019,** *365*, 463-472.
(10) Nagao, R.; Kato, K.; Suzuki, T.; Ifuku, K.; Uchiyama, I.; Kashino, Y.; Dohmae, N.; Akimoto, S.; Shen, J. R.; Miyazaki, N., *et al.* Structural basis for energy harvesting and dissipation in a diatom PSII-FCPII supercomplex. *Nature Plants* **2019,** *5*, 890-901.
(11) Kok, B.; Forbush, B.; McGloin, M. Cooperation of Charges in Photosynthetic O_2 Evolution.1. A Linear 4 Step Mechanism. *Photochem. Photobiol.* **1970,** *11*, 457-475.
(12) Matsukawa, T.; Mino, H.; Yoneda, D.; Kawamori, A. Dual-mode EPR study of new signals from the S_3-state of oxygen-evolving complex in photosystem II. *Biochemistry* **1999,** *38*, 4072-4077.

(13) Campbell, K. A.; Gregor, W.; Pham, D. P.; Peloquin, J. M.; Debus, R. J.; Britt, R. D. The 23 and 17 kDa extrinsic proteins of photosystem II modulate the magnetic properties of the S_1-state manganese cluster. *Biochemistry* **1998,** *37*, 5039-5045.
(14) Banerjee, G.; Ghosh, I.; Kim, C. J.; Debus, R. J.; Brudvig, G. W. Substitution of the D1-N87 site in photosystem II of cyanobacteria mimics the chloride-binding characteristics of spinach photosystem II. *J. Biol. Chem.* **2018,** *293*, 2487-2497.
(15) Cullen, M.; Ray, N.; Husain, S.; Nugent, J.; Nield, J.; Purton, S. A highly active histidine-tagged *Chlamydomonas reinhardtii* Photosystem II preparation for structural and biophysical analysis. *Photochem. Photobiol. Sci.* **2007,** *6*, 1177-1183.
(16) Boussac, A.; Kuhl, H.; Un, S.; Rogner, M.; Rutherford, A. W. Effect of near-infrared light on the S_2-state of the manganese complex of photosystem II from *Synechococcus elongatus*. *Biochemistry* **1998,** *37*, 8995-9000.
(17) Boussac, A. Temperature dependence of the high-spin S_2 to S_3 transition in Photosystem II: Mechanistic consequences. *Biochim. Biophys. Acta* **2019,** *1860*, 508-518.
(18) Boussac, A.; Ugur, I.; Marion, A.; Sugiura, M.; Kaila, V. R. I.; Rutherford, A. W. The low spin - high spin equilibrium in the S_2-state of the water oxidizing enzyme. *Biochim. Biophys. Acta* **2018,** *1859*, 342-356.
(19) Ioannidis, N.; Nugent, J. H. A.; Petrouleas, V. Intermediates of the S_3 state of the oxygen-evolving complex of photosystem II. *Biochemistry* **2002,** *41*, 9589-9600.
(20) Ioannidis, N.; Petrouleas, V. Decay products of the S_3 state of the oxygen-evolving complex of photosystem II at cryogenic temperatures. Pathways to the formation of the S=7/2 S_2 state configuration. *Biochemistry* **2002,** *41*, 9580-9588.
(21) Pantazis, D. A.; Ames, W.; Cox, N.; Lubitz, W.; Neese, F. Two interconvertible structures that explain the spectroscopic properties of the oxygen-evolving complex of photosystem II in the S_2 state. *Angew. Chem. Int. Ed. Engl.* **2012,** *51*, 9935-9940.
(22) Corry, T. A.; O'Malley, P. J. Molecular Identification of a High-Spin Deprotonated Intermediate during the S_2 to S_3 Transition of Nature's Water-Oxidizing Complex. *J. Am. Chem. Soc.* **2020,** *142*, 10240-10243.
(23) Taguchi, S.; Noguchi, T.; Mino, H. Molecular Structure of the S_2 State with a g = 5 Signal in the Oxygen Evolving Complex of Photosystem II. *J. Phys. Chem. B* **2020,** *124*, 5531-5537.
(24) Debus, R. J. Evidence from FTIR Difference Spectroscopy That D1-Asp61 Influences the Water Reactions of the Oxygen-Evolving Mn_4CaO_5 Cluster of Photosystem II. *Biochemistry* **2014,** *53*, 2941-2955.
(25) Ono, T.; Zimmermann, J. L.; Inoue, Y.; Rutherford, A. W. EPR evidence for a modified S-state transition in chloride-depleted Photosystem II. *Biochim. Biophys. Acta* **1986,** *851*, 193-201.
(26) vanVliet, P.; Rutherford, A. W. Properties of the chloride-depleted oxygen-evolving complex of photosystem II studied by electron paramagnetic resonance. *Biochemistry* **1996,** *35*, 1829-1839.
(27) Pokhrel, R.; Brudvig, G. W. Oxygen-evolving complex of photosystem II: correlating structure with spectroscopy. *Phys. Chem. Chem. Phys.* **2014,** *16*, 11812-11821.
(28) Cox, N.; Rapatskiy, L.; Su, J. H.; Pantazis, D. A.; Sugiura, M.; Kulik, L.; Dorlet, P.; Rutherford, A. W.; Neese, F.; Boussac, A., *et al.* Effect of Ca^{2+}/Sr^{2+} Substitution on the Electronic Structure of the Oxygen-Evolving Complex of Photosystem II: A Combined Multifrequency EPR, ^{55}Mn- ENDOR, and DFT Study of the S_2 State. *J. Am. Chem. Soc.* **2011,** *133*, 3635-3648.

(29) Mino, H.; Nagashima, H. Orientation of Ligand Field for Dangling Manganese in Photosynthetic Oxygen-Evolving Complex of Photosystem II. *J. Phys. Chem. B* **2020,** *124*, 128-133.
(30) Suga, M.; Akita, F.; Hirata, K.; Ueno, G.; Murakami, H.; Nakajima, Y.; Shimizu, T.; Yamashita, K.; Yamamoto, M.; Ago, H., *et al.* Native structure of photosystem II at 1.95 Å resolution viewed by femtosecond X-ray pulses. *Nature* **2015,** *517*, 99-103.
(31) Isobe, H.; Shoji, M.; Yamanaka, S.; Umena, Y.; Kawakami, K.; Kamiya, N.; Shen, J. R.; Yamaguchi, K. Theoretical Illumination of Water-inserted Structures of the $CaMn_4O_5$ cluster in the S_2 and S_3 States of Oxygen-Evolving Complex of photosystem II: Full Geometry Optimizations by B3LYP Hybrid Density Functional. *Dalton Trans.* **2012,** *41*, 13727-13740.
(32) Zlatar, M.; Gruden, M.; Vassilyeva, O. Y.; Buvaylo, E. A.; Ponomarev, A. N.; Zvyagin, S. A.; Wosnitza, J.; Krzystek, J.; Garcia-Fernandez, P.; Duboc, C. Origin of the Zero-Field Splitting in Mononuclear Octahedral Mn-IV Complexes: A Combined Experimental and Theoretical Investigation. *Inorg. Chem.* **2016,** *55*, 1192-1201.
(33) Corry, T. A.; O'Malley, P. J. Proton Isomers Rationalize the High and Low Spin Forms of the S_2 State Intermediate in the Water Oxidising Reaction of Photosystem 2. *J. Phys. Chem. Lett.* **2019**.
(34) Yamaguchi, K.; Isobe, H.; Shoji, M.; Yamanaka, S.; Okumura, M. Theory of chemical bonds in metalloenzymes XX: magneto-structural correlations in the $CaMn_4O_5$ cluster in oxygen-evolving complex of photosystem II. *Molecular Physics* **2016,** *114*, 519-546.
(35) Suga, M.; Akita, F.; Sugahara, M.; Kubo, M.; Nakajima, Y.; Nakane, T.; Yamashita, K.; Umena, Y.; Nakabayashi, M.; Yamane, T., *et al.* Light-induced structural changes and the site of O=O bond formation in PSII caught by XFEL. *Nature* **2017,** *543*, 131-135
(36). Kern, J.; Chatterjee, R.; Young, I. D.; Fuller, F. D.; Lassalle, L.; Ibrahim, M.; Gul, S.; Fransson, T.; Brewster, A. S.; Alonso-Mori, R., *et al.* Structures of the intermediates of Kok's photosynthetic water oxidation clock. *Nature* **2018,** *563*, 421- 425.
(37) Suga, M.; Akita, F.; Yamashita, K.; Nakajima, Y.; Ueno, G.; Li, H. J.; Yamane, T.; Hirata, K.; Umena, Y.; Yonekura, S., *et al.* An oxyl/oxo mechanism for oxygen-oxygen coupling in PSII revealed by an x-ray free-electron laser. *Science* **2019,** *366*, 334-338.
(38) Shen, J. R.; Inoue, Y. Binding and functional properties of two new extrinsic components, cytochrome-C-550 and a 12-kDa protein, in cyanobacterial Photosystem II. *Biochemistry* **1993,** *32*, 1825-1832.
(39) Adachi, H.; Umena, Y.; Enami, I.; Henmi, T.; Kamiya, N.; Shen, J. R. Towards structural elucidation of eukaryotic photosystem II: Purification, crystallization and preliminary X-ray diffraction analysis of photosystem II from a red alga. *Biochim. Biophys. Acta* **2009,** *1787*, 121-128.
(40) Tomita, M.; Ifuku, K.; Sato, F.; Noguchi, T. FTIR Evidence That the PsbP Extrinsic Protein Induces Protein Conformational Changes around the Oxygen-Evolving Mn Cluster in Photosystem II. *Biochemistry* **2009,** *48*, 6318-6325.
(41) Nagao, R.; Tomo, T.; Noguchi, T. Effects of Extrinsic Proteins on the Protein Conformation of the Oxygen-Evolving Center in Cyanobacterial Photosystem II As Revealed by Fourier Transform Infrared Spectroscopy. *Biochemistry* **2015,** *54*, 2022-2031.